Fermi National Accelerator Laboratory

FERMILAB-TM-2016

On the Effects of Fringe Fields in the Recycler Ring

F. Méot

Fermi National Accelerator Laboratory
P.O. Box 500, Batavia, Illinois 60510

August 1997

Operated by Universities Research Association Inc. under Contract No. DE-AC02-76CH03000 with the United States Department of Energy

Disclaimer

Distribution

On the effects of fringe fields in the Recycler ring

F. Méot*
Fermi National Accelerator Laboratory
P.O. Box 500, Batavia, Illinois 60510

August 15, 1997

Abstract

Effects of the combined function dipole fringe fields on machine parameters are investigated by means of stepwise ray-tracing.

*On leave from CEA/DSM-Saclay, France

Contents

1 Introduction

Limited tuning range (with phase trombone) in the Recycler ring [1] makes it worth disclosing all possible sources of tune shifts and other alteration of machine parameters. In this respect, the present study aims at describing effects of fringe fields present in the combined function dipoles. It is performed by means of the ray-tracing code Zgoubi which is based on stepwise solution of Lorentz equation by a method of Taylor series. Aspects of the code relevant with this study are made clear below, more details can be found in Ref. [2]. A major feature of the method, of strong interest in precision tracking as will be discussed later, is its ability to handle arbitrary magnetic fields with intrinsically strong symplecticity. These issues have already been subject to meticulous investigations in previous works, e.g. on the Saturne synchrotron [3] and on the LHC ring [4]. For instance the fractional tunes in the sharp edge field model are recovered at better than 10^{-4} in both cases, Saturne (105 m perimeter) : $\nu_x/\nu_y = 3.638574/3.620744$ from matrix transport, $\nu_x/\nu_y = 0.638564/0.620667$ from ray-tracing, and LHC (26700 m perimeter) : $\nu_x/\nu_y = 63.28000/63.31000$ from matrix transport, $\nu_x/\nu_y = 0.28006/63.31007$ from ray-tracing. Such results give confidence in the ability of the ray-tracing method to, on the one hand handle with precision such perturbations as end fields, on the other hand provide accurate computation of machine parameters.

2 Ray-tracing in the Recycler combined function dipoles

2.1 Multipole field

The rectangular combined function dipoles of the Recycler can be simulated with the built-in Multipole procedure of Zgoubi. The field and derivatives necessary for the Taylor-series based stepwise resolution of the Lorentz equation [2] are drawn from regular 3D scalar potential model [5] which in the case of the dipole through sextupole components takes the respective forms

$$V_1(z,x,y) = \alpha_{1,0}(z)y - \frac{\alpha_{1,0}^{(2)}(z)}{8}(x^2+y^2)y + \frac{\alpha_{1,0}^{(4)}(z)}{192}(x^2+y^2)^2y - ... \quad (1)$$

$$V_2(z,x,y) = \alpha_{2,0}(z)xy - \frac{\alpha_{1,0}^{(2)}(z)}{12}(x^2+y^2)xy + \frac{\alpha_{1,0}^{(4)}(z)}{384}(x^2+y^2)^2xy - ... \quad (2)$$

$$V_3(z,x,y) = \frac{\alpha_{3,0}(z)}{3}(3x^2-y^2)y - \frac{\alpha_{3,0}^{(2)}(z)}{48}(3x^4+2x^2y^2-y^4)y + ... \quad (3)$$

where the z, x, y coordinates are respectively longitudinal, transverse horizontal and vertical, $\alpha_{n,0}(z)$ $(n = 1,2,3)$ describes the longitudinal form $(x = y = 0)$(see Section 2.2) and $\alpha_{n,0}^{(2q)} = d^{2q}\alpha_{n,0}/dz^{2q}$. Note that, in the magnet body or as well when using a sharp edge field model, $d^{2q}\alpha_{n,0}/dz^{2q} \equiv 0$ (whatever $q \neq 0$) and hence the field and derivatives derive from the simplified potentials

$$V_1(x,y) = G_1y,\ V_2(x,y) = G_2xy,\ V_3(x,y) = G_3(3x^2-y^2)y/3 \quad (4)$$

where the transverse gradients G_n are constant.

2.2 Fringe field model

The field fall-off on axis at dipole ends orthogonally to the effective field boundary (*EFB*) is modeled by [6, p. 240]

$$\alpha_{n,0}(d) = \frac{G_n}{1+exp[P(d)]}\ ,\ \ P(d) = C_0 + C_1\frac{d}{\lambda_n} + C_2(\frac{d}{\lambda_n})^2 + C_3(\frac{d}{\lambda_n})^3 \quad (5)$$

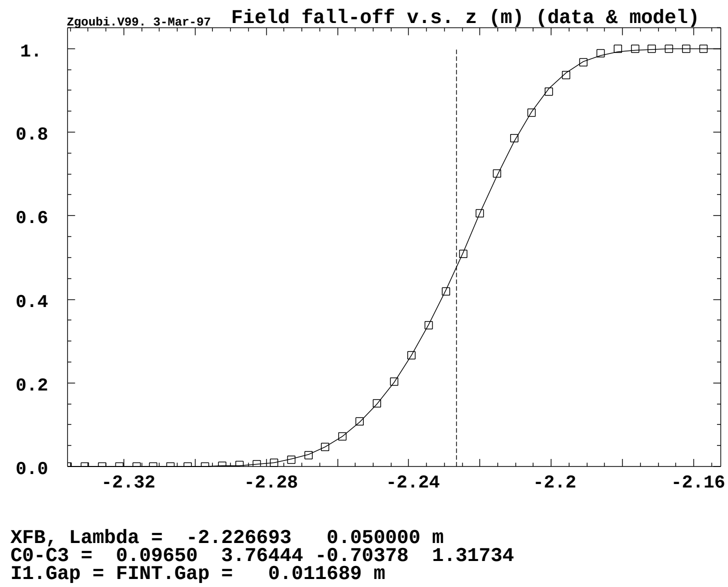

Figure 1: Field fall-off used for the simulation of the Recycler combined function dipole ends (the $\alpha_{1,0}$ form factor in Eq. (1)). The coefficients λ_1, $C_0 - C_3$ obtained by matching field data (squares) with the Enge model (Eq. 5) are as displayed here and provide the solid line fall-off. The $I1 \cdot gap$ value as used in MAD simulations is also indicated. *XFB* is the position of the *EFB*, symbolized by the vertical dashed line.

where d is the distance to the *EFB*, and the numerical coefficients λ_n, $C_0 - C_3$ are determined from prior matching with numerical fringe field data. This is usually done in such a way that $\lambda_1 \approx$ *gap size* in which case one can take identical values $C_{0,1,2,3}$ for $n = 1 - 3$ while $\lambda_{2,3} \approx \lambda_1/2,\ \lambda_1/3$. The λ_n can be varied at will to possibly change or test the effect of the fall-off gradient, without affecting the position of the *EFB* (i.e., without any effect on the magnetic length of the dipole). However we will set $\lambda_1 = \lambda_2 = \lambda_3 =$ *gap size* for the combined function dipoles whose shape is closer to a regular dipole geometry. The fringe field used here is shown in Fig. 1 [7] which also displays the corresponding matching Enge coefficients and the integral parameter $I1 \cdot gap = \int \alpha_{n,0}(z)(1 - \alpha_{n,0}(z))dz$ as used in further MAD simulations [8, 9].

3 Sextupole free model

3.1 Magnet alignment ; orbit offset

Just like in the real world the magnets need be aligned in the Zgoubi data file. This is done by specifying the position of the design orbit at magnet entrance and exit, which can be worked out as follows (see also [10]).

3.1.1 Sharp edge field model

Let (O,x,y,z) be the reference frame of the magnet (Fig. 2). Due to the transverse index $n = (\rho/B)(dB/dx)$ a particle traversing the rectangular combined function dipole experiences a non-constant bending, contrary to what would occur in a bent dipole with field index $(\rho/B)(dB/d\rho)$. The entrance position x_{off} in the dipole must therefore be defined in such a way as to ensure the required total deviation in the Recycler magnet $\theta = 2\pi/(301 + \frac{1}{3})$. The combined function dipole

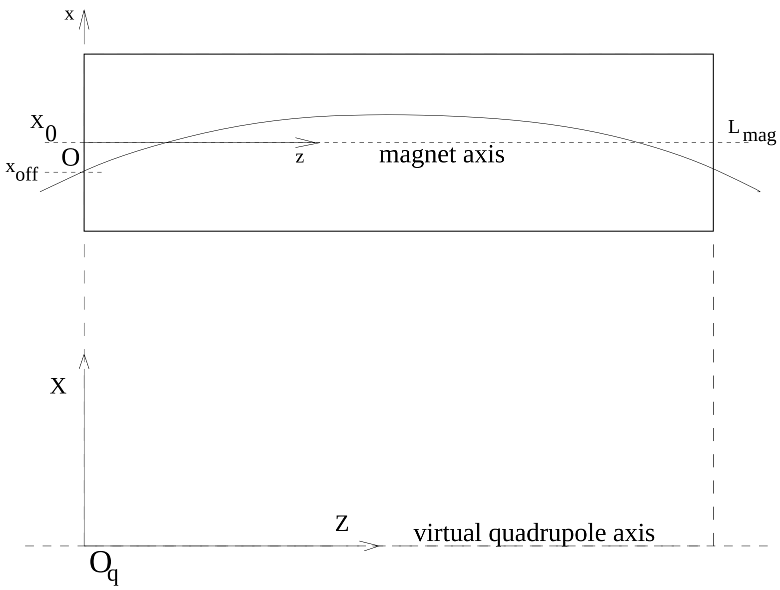

Figure 2: Referentials in the combined function dipole and in the equivalent quadrupole in the $K > 0$ case (the trajectory is in $X < 0$ regions when $K < 0$).

can conveniently be viewed as a simple quadrupole traversed far off axis ; the entrance coordinates X_{off}, X'_{off} of the design orbit in the reference frame (O_q,X,Y,Z) (Fig. 2) therefore verify (second order effects are explicitly ignored)

$$\begin{pmatrix} X(Z) \\ X'(Z) \end{pmatrix} = \begin{pmatrix} cos(Z\sqrt{K}) & \frac{1}{\sqrt{K}}sin(Z\sqrt{K}) \\ -\sqrt{K}sin(Z\sqrt{K}) & cos(Z\sqrt{K}) \end{pmatrix} = \begin{pmatrix} X_{off} \\ X'_{off} \end{pmatrix}, \tag{6}$$

with $K = (1/B\rho)(dB/dx)$ =quadrupole strength, $(') = d/dZ$, $B\rho$ =particle rigidity. Symmetry imposes two (compatible) constraints $X(Z \equiv L_{mag}) = X_{off}$ and $-X'(Z \equiv L_{mag}) = X'_{off} = \theta/2$ which put in Eq. (6) lead to

$$X_{off} = \frac{S}{1-C}X'_{off} = \frac{S}{1-C}\;\frac{\theta}{2} = \frac{1+C}{KS}\;\frac{\theta}{2} \approx (1 - \frac{KL^2}{12})\frac{\theta}{KL} \quad (K \gtrless 0) \tag{7}$$

In these expressions we take $C = cos(L\sqrt{K})$, $S = \frac{1}{\sqrt{K}}sin(L\sqrt{K})$ with $L = \rho\theta$ instead of L_{mag} ; this scaling is to account for the actual magnetic length that provides θ deviation, with $\rho = L_{mag}/(2sin\theta/2)$ and $L_{mag} = 4.4958$ m is the dipole length (the difference is however small, less than 2 10^{-5} relative). On the other hand the reference axis (Oz) of the dipole coincides with the field value $B(X_0) \equiv B_0 = B\rho/\rho$ and is distant $X_0 = B_0/(dB/dx) = B_0/KB\rho = \theta/KL$ from the quadrupole axis (O_qZ). The design orbit at magnet entrance is therefore offset w.r.t. the (Oz) axis by the amount

$$x_{off} = X_{off} - X_0 = \big(\frac{S}{2\sqrt{K}(1-C)} - \frac{1}{KL}\big)\;\theta, \qquad K \gtrless 0 \tag{8}$$

The field at offset is

$$B_{off} = KB\rho X_{off} = B\rho\frac{1+C}{S}\frac{\theta}{2} \tag{9}$$

and the bending radius is

Table 1: Parameters entering the simulation of the Recycler combined function magnets, corresponding to the deviation $\theta = 2\pi/(301+\frac{1}{3})$ in ARCF/D dipoles and 2/3 that value in DISF/D. Field values are for 8 GeV protons ($B\rho = 29.650\ Tm$) ; in particular the design field is $B_0 = 0.137513$ T corresponding to $\rho = 215.617$.

Dipole type	Quad strength K ($10^{-2}m^{-2}$)	Orbit offset x_{off} (10^{-3} m)	Field at offset B_{off} (T)	Adjusted offset (with fringe field) x^*_{off} (10^{-3}m)
ARCF	1.151435	-7.8426	0.1348358	-7.8371
ARCD	-1.111505	-7.7828	0.1400782	-7.7848
DISF	2.306099	-3.4841	0.1351311	-3.4814
DISD	-2.306099	-3.4601	0.1398792	-3.4589

$$\rho_{off} = B\rho/B_{off} = \frac{2S}{(1+C)\theta} \tag{10}$$

Note that, the motion can be expressed in the (O,x,y,z) frame by introducing $X(Z) = x(z) + X_0 = x(z) + \theta/KL$ and $X'_{off} = \theta/2$ in Eq. (6) which leads to

$$x(z) + \frac{\theta}{KL} = \frac{\theta}{2}\{\frac{1+C}{KS}cos(z\sqrt{K}) + \frac{sin(z\sqrt{K})}{\sqrt{K}}\} \quad (K\gtrless 0) \tag{11}$$

as discussed in Ref. [11]. Table 1 gives the offsets computed from the strength K and deviation θ for all four dipole types ARCF, ARCD, DISF and DISD of the Recycler ring (after MAD files [9], see App. C), as utilized in Zgoubi data files (App. A).

3.1.2 Fringe field model

In presence of the dipole fringe field described in Section 2.2 a particle placed on the design orbit far upstream of the dipole is expected to leave the design orbit when crossing the entrance fringe field and, contrary to what would occur in a pure dipole field Ref. [6, p. 242], will not return to the design orbit downstream the exit *EFB* because of the field index. The weakness of this combined effect *fringe field + transverse index* is shown in col. 5 of Table 1 in terms of the adjusted offset x^*_{off} (obtained by numerical Fit procedure [2]) providing identical entrance and exit coordinates and exact θ deviation for a reference particle : this adjustment is negligible, less than 5 μm. Note that, as a consequence the effect on the machine closed orbit is weak as well, as shown in Section 3.3.1.

3.2 Particle motion in a single dipole

The design orbit in the combined function magnet as obtained from ray-tracing of a particle entering an ARCF dipole at x_{off} (Eq. 8) is shown in Fig. (3) together with the magnetic field along, including the end fringe fields of Fig. (1). The ray-tracing shows that the path length is $L = 4.495881$ m for the total deviation $\theta = 2\pi/(301+\frac{1}{3})$, which coincides with the circular path length $\rho\theta$ with $\rho = L_{mag}/(2sin\theta/2) = 215.61658$ m (corresponding to the pure dipole field value $B_0 = B\rho\theta/L = 0.137513T$ T for $B\rho = 29.650\ Tm$). The difference between the circular path and the actual cosine-like trajectory (Eq. 11) is discussed in App. B. The sagitta is obtained from (Eqs. 7, 8)

$$x(z) - x_{off} = \{(cos(z\sqrt{K}) - 1)\frac{1+C}{KS} + \frac{sin(z\sqrt{K})}{\sqrt{K}}\}\frac{\theta}{2} \quad (K\gtrless 0) \tag{12}$$

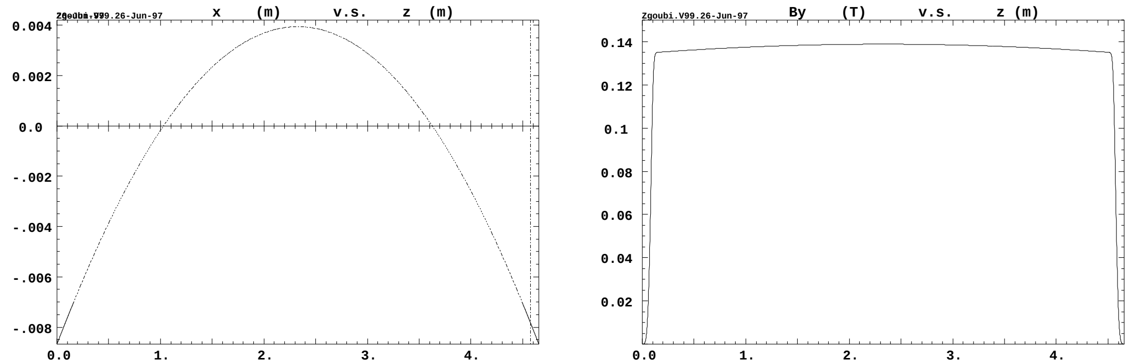

Figure 3: Left : horizontal trajectory of a particle entering ARCF at x_{off} under incidence $\theta/2$. Fringe fields do not make sensible difference. This path materializes the effective design orbit in the dipole. Right : magnetic field along the design orbit of an ARCF dipole including field fall-offs at both ends. The non constant field in the body is a combined effect of quadrupole index and bent trajectory. The vertical dashed lines represent the EFB's.

with $z = L_{mag}/2$ which leads to respectively $1.1775\,10^{-2}$ m and $1.1664\,10^{-2}$ m in ARCF and ARCD. As a comparison, the ray-tracing with sharp edge model provides identical values.

3.2.1 Horizontal motion with fringe fields

As shown in Ref. [6, pp. 243-244] the fringe field of a pure dipole does not induce any change in horizontal focusing, i.e., incoming parallel rays exit parallel ; this still holds in presence of the low field index in the Recycler dipole, as seen from the transfer matrices in Table 2 : the change of horizontal transfer coefficient from sharp edge to fringe field configuration is less than $5\ 10^{-4}$ (relative). Another manifestation of fringe fields, of order zero, is to produce a displacement of the design orbit inside the dipole with maximum amplitude [6, p. 244]

$$\Delta x \approx I1 \cdot gap^2/\rho_{off} \tag{13}$$

for instance in an ARCF (ARCD) dipole $\rho_{off} = B\rho/B_{off} \approx 219.8$ m (211.6 m) (Eq. 10 and Table 1), $gap = 5\ 10^{-2}$ m and $I1 \cdot gap \approx 1.17\,10^{-2}$ m (Fig. 1) which leads to $\Delta x \approx 2\ 10^{-6}$ m ($3\ 10^{-6}$ m). Even combined with the transverse index this results in very small distortion of the design orbit, as shown in Subsection 3.1.2 ; as a comparison with what precedes, the sagitta are unchanged (respectively $1.1775\ 10^{-2}$ m and $1.1664\ 10^{-2}$ m in ARCF and ARCD). Considering such weakness of fringe field effects to zero and first order, possible higher order effects on the geometry can be neglected.

3.2.2 Vertical motion with fringe fields

The vertical first order term due to the wedge angle is $\tan(\theta/2 - \psi)/\rho_{off}$ where ψ is the correction term to the wedge angle which accounts for the effect of the fringe field ($\psi = 0$ with sharp edge) and is given by [6, p. 247]

$$\psi = \frac{I1 \cdot gap}{\rho_{off}}(1 + sin^2\theta/2) \approx \frac{I1 \cdot gap}{\rho_{off}} \tag{14}$$

Given $\rho_{off} \approx 215$ m, $I1 \cdot gap \approx 1.17\,10^{-2}$ m (Fig. 1) and with $\theta/2 \approx 10^{-3}$ rad, it comes $\psi \approx 5\,10^{-3}\,\theta/2$ in ARCF/D dipoles. In other words the vertical focusing is but weakly affected by the fringe fields, as confirmed by transfer matrix calculations (Table 2).

Table 2: First order transfer matrices in the ARCF dipole (this is a sample, results are similar for the other types of dipoles). Note that, in ray-tracing with sharp edge field model the wedge effect in the vertical motion is simulated by a wedge kick applied independently to each particle at entrance and exit EFB's. MAD simulations are given in App. C for comparison. The agreement between ray-tracing and MAD in the sharp edge model is excellent : differences in transfer coefficient values do not exceed 1-2 units on the last digit ; such small differences lead to less than 3.2 10^{-4} difference in fractional tune values as shown in Section 3.3.2 (Table 3). This is no longer the case in presence of fringe fields. The absence of any effect of the adjustment to x^*_{off} is seen by comparison of the last two matrices.

```
ARCF
  Sharp Edge

       0.885868    4.323187    0.000000    0.000000
      -0.049787    0.885868    0.000000    0.000000
       0.000000    0.000000    1.118420    4.672315
       0.000000    0.000000    0.053692    1.118420

  Fringe field  and x_off = 7.8426319361E-01

       0.885819    4.323285    0.000000    0.000000
      -0.049806    0.885818    0.000000    0.000000
       0.000000    0.000000    1.118475    4.672209
       0.000000    0.000000    0.053719    1.118475

  Fringe field  and x_off* = 7.83711560E-01

       0.885818    4.323285    0.000000    0.000000
      -0.049806    0.885818    0.000000    0.000000
       0.000000    0.000000    1.118475    4.672209
       0.000000    0.000000    0.053719    1.118475
```

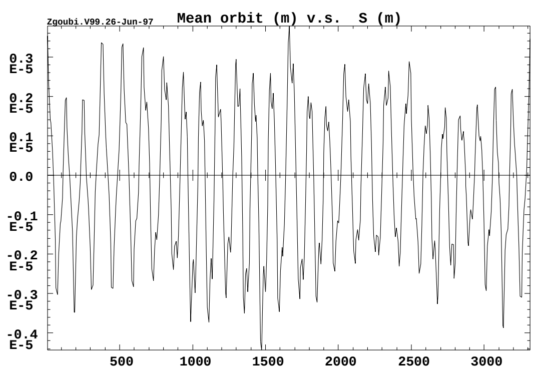

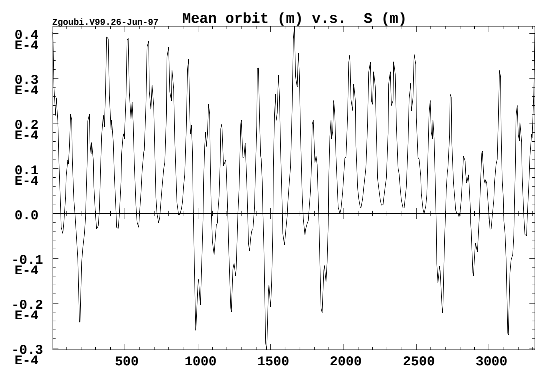

Figure 4: *Left* : closed orbit in the sharp model along the ring as recorded at HMON and VMON beam position monitors. The horizontal axis displays monitor numbers. *Right* : closed orbit along the machine under the effect of fringe fields. Entrance offset is x_{off} in both cases (col. 3 of Table 1).

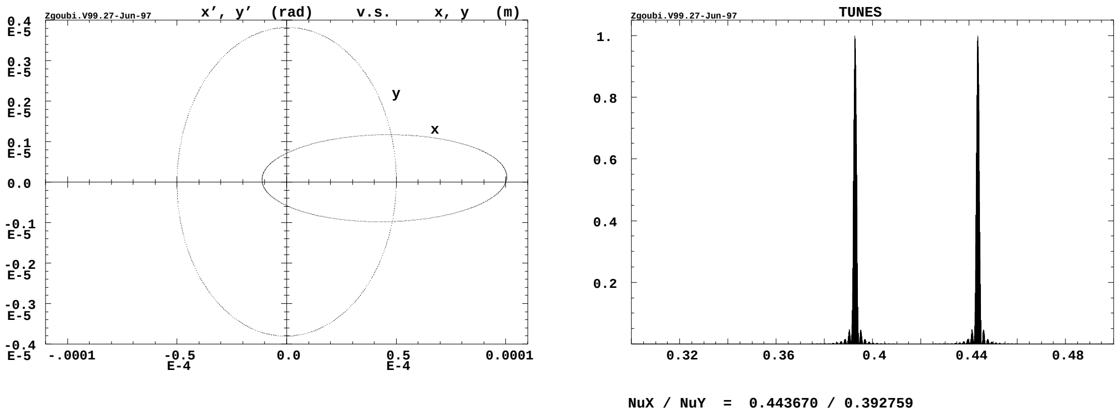

Figure 5: *Left plot* : 600 turns horizontal and vertical phase space ellipses at the beginning of the structure, from ray-tracing with fringe field model ; the particle is launched on the invariants $\epsilon_{x,y}/\pi \approx 10^{-10}$ m.rad. the horizontal closed orbit is a few tens of micrometers because the alignment value x_{off} is used (Eq. (7) and col. 3 of Table 1) ; using x^*_{off} instead (col. 5 of Table 1) would reduce it by about one order of magnitude. *Right plot* : Machine tunes in fringe field model, from Fourier analysis of the 600-turn tracking of the left plot. The limited sampling is cause of the non zero line width.

3.3 Machine parameters

3.3.1 Closed orbit

Figure 4 shows the very small horizontal closed orbit excursion ($\approx \pm 4\ \mu m$) provided by the ray-tracing in the sharp edge field model with design field $B_0 = 0.137513T$ T and with offset value x_{off} from the cosine-like trajectory model (col. 3 of Table 1 and Eq. (8)). The Figure also shows the negligible effect of fringe fields, as expected from Section 3.1 : the so increased excursion does not exceed $\pm 0.04\ 10^{-3}$ m ; as shown in col. 5 of Table 1 x_{off} would have to be adjusted by less than 5.5 μm in order to cancel it. In both cases the closed orbit is calculated from a 100-turn average particle position at HMON and VMON monitors located as in MAD files [9].

3.3.2 Tunes

The tune values are computed either from a calculation of the full turn first order transfer matrix obtained by ray-tracing of a set of paraxial rays over one machine turn, or from multiturn ray-tracing and Fourier analysis of a single paraxial particle (launched on the invariants $\epsilon_x/\pi \approx \epsilon_y/\pi \approx 1.810^{-10}$ m·rad at the start of the structure). Both methods give results similar at better than 5 10^{-6} (absolute value) such as displayed in Table 3.

In the 1-turn matrix calculation, the symplecticity is checked through the horizontal and vertical determinants. Namely, these differ from 1 by less than 10^{-8} in all tune calculations. In the 600-turn tracking and Fourier analysis the symplecticity is checked through the smear of the invariants as obtained by an ellipse matching of the phase space plots ; the smear is negligible, it does not exceed $\sigma(\epsilon_{x,z}/\pi) \approx 5\ 10^{-3}$ m.rad (r.m.s.) in all tune calculations. Figure (5) shows an example of the Fourier analysis data and post-processing in the fringe field model case.

MAD simulations are given for comparison (see also App. C). Note that, for the sake of consistency these include some changes on MAD data namely, on the one hand RBEND with length $L = \rho\theta$ instead of L_{mag}, on the other hand a corrected wedge angle so as to allow for the particular bend radius values at dipole ends - this is discussed in App. D.

Table 3 deserves some comments.

• The differences in tune from sharp edge to fringe field model observed with ray-tracing fit the difference in the focusing terms in the transfer matrix (R_{21}, R_{43} coefficients, Table 2), as estimated from $\Delta\nu = (1/4\pi)\int \beta\Delta K ds$ with $\beta \approx 50$ m and $\Delta(KL) \approx 2\ 10^{-5}$ in about 170 dipoles.

• As to the effect of fringe fields on the horizontal tune, they do not exist in matrix transport, and they remain to be understood as to the ray-tracing method ($\approx 1.5\ 10^{-2}$ difference with MAD) It has been checked that they are not due to the non-linearities introduced by the second order derivative $d^2\alpha_{1,0}/dz^2$ of the longitudinal form factor in the fringe field (Eq. 1), whose effect is in fact negligible. However the ray-tracing method is extremely precise, and utilizes the right model for the straight combined function dipole, which gives it more credit.

• As to the vertical tunes they also differ by $\approx 1.8\ 10^{-2}$ in fringe field model (in agreement with the $\approx 2.5\ 10^{-5}$ difference in the R_{43} transfer coefficient as mentioned above). In order to obtain similar value with MAD, it appears that the effective parameter in this respect, $I1 \cdot gap$, would have to be changed by a non physical amount, therefore the reason for the difference has to be looked for somewhere else.

Table 3: Machine tunes obtained by ray-tracing of paraxial rays. Tunes from MAD calculations are given in rows 3,4, for comparison. The agreement in the sharp edge case is $\approx 3.3\ 10^{-4}$ (absolute) in both planes w.r.t. "modified" (App. D) MAD simulation, which means that further comparisons are seated on a satisfactory basis.

	Horizontal tune	Vertical tune
Ray-tracing		
Sharp edge	0.428015	*0.410913*[a]
Fringe field with x_{off}	0.443671	0.392760
Fringe field with x^*_{off}	0.443670	0.392762
MAD, modified[b]		
Sharp edge	25.428346	24.411267
Fringe field	25.428346	24.410859
MAD, original[c]		
Sharp edge	25.42700	24.409949
Fringe field	25.42700	24.408890

[a] Absence of fringe field is compensated by vertical wedge kick
[b] RBEND with $L = \rho\theta$ and modified wedge angles (Apps. C, D)
[c] See App. C [9]

Chromaticities

Chromaticities are computed from tunes of particles on off-momentum closed orbit. We take $\delta p/p = 10^{-3}$ with $x_{ch} = \eta_x \delta p/p \approx 1.975\ 10^{-3}$ m and $x'_{ch} = \eta'_x \delta p/p \approx 0.8\ 10^{-6}$ rad at the start of the structure [9], which results in what follows :

- Sharp edge model :
With sharp edge field model we obtain $\nu_x/\nu_y = 0.396606$ / 0.379555 which, given the on-momentum tunes 0.428015 / 0.410913 (Table 3) leads to $\delta\nu_{x,y}/\delta p/p$, $\delta\nu_{x,y}/\delta p/p =$ -31.4, -31.4, identical to MAD values.

- Fringe field model :
In presence of fringe fields we get $\nu_x/\nu_y = 0.41245$ / 0.36144 which, given the on-momentum tunes

0.44367 / 0.39276 (Table 3) leads to $\delta\nu_{x,y}/\delta p/p$, $\delta\nu_{x,y}/\delta p/p$ = -31.2, -31.3 which does not differ significantly from the sharp edge model values above.

3.3.3 Twiss functions

Elliptical matching of the phase space plots (Fig. 5) provide the Twiss function values $\beta_x = 51.927$ m/rad, $\alpha_x = -0.0332$, $\beta_y = 13.123$ m/rad, $\alpha_y = -0.00864$ in the fringe field case, very close to first order simulations with MAD (App. C).

4 Addition of the sextupole index

4.1 Feed down to dipole

In the sharp edge field model in order to get the right deviation $\theta = 2\pi/(301 + \frac{1}{3})$ in the combined function dipoles, under the effect of sextupole index the design orbit offsets x_{off} have to be tuned. This is done by means of a numerical fitting procedure in Zgoubi [2], and provides the values as collected in Table 4. As can be checked the adjustment is very weak (x_{off} is changed at maximum by $\approx 6\ \mu m$ in ARCF and $\approx 12.7\ \mu m$ in ARCD) which in particular entails unchanged sagitta w.r.t. the pure quadrupole case, whether the sharp edge or fringe field model is used (respectively 1.1775 10^{-2} m and 1.1664 10^{-2} m in ARCF and ARCD, as in Section 3.2).

Table 4: Offset values at entrance in ARCF and ARCD necessary for obtaining $\theta = 2\pi/(301 + \frac{1}{3})$ deviation. All other parameters are as in the pure quadrupole case (Table 1). For comparison, offsets in the pure quadrupole case, sharp edge field model, were respectively $x_{off} = -7.8426\ 10^{-3}$ m and $-7.7828\ 10^{-3}$ m in ARCF and ARCD (Table 1).

Dipole type	Sextu strength H ($10^{-2} m^{-3}$)	Adjusted offset (Sharp edge) (10^{-3} m)	Adjusted offset (Fringe field) (10^{-3} m)
ARCF	1.155289	-7.8487	-7.8433
ARCD	-1.942155	-7.7935	-7.7955

4.2 Closed orbit

The horizontal closed orbit excursion stays practically unchanged when sextupole indices are switched on in ARCF and ARCD dipoles (with offsets x_{off} as in the pure quadrupole case, respectively $-7.8426\ 10^{-3}$ m and $-7.7828\ 10^{-3}$ m). This is clear from comparison of the ensuing Fig. (6) with the pure quadrupole cases displayed in Fig. (4). Namely, the horizontal excursions remain $\approx \pm 4\ \mu m$ in sharp edge model and $\approx \pm 40\ \mu m$ in fringe field model.

4.3 Tunes

Table 5 gives tune values computed from one-turn first order transfer matrix obtained by ray-tracing of a set of paraxial rays. Comparison with Table 3 shows that ν_x/ν_y are increased by 2.2 10^{-3}/3.1 10^{-3}. This can be interpreted in terms of sextupole feed down (App. E).
Chromaticities

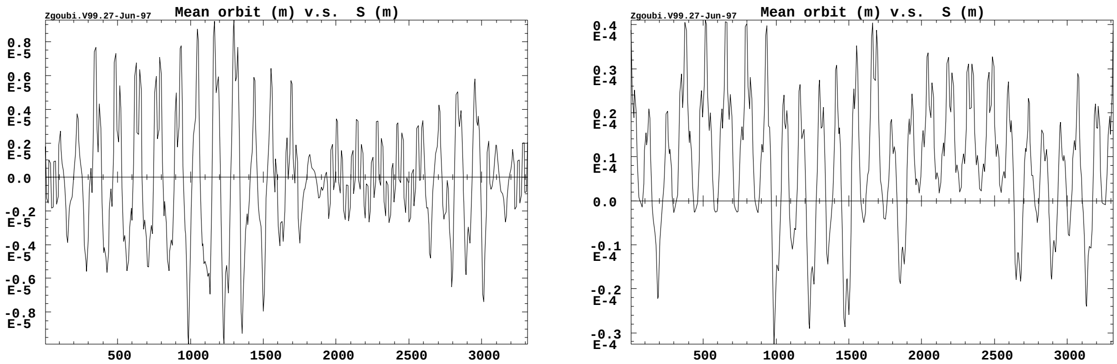

Figure 6: *Left plot* : closed orbit in the sharp edge field model along the machine at HMON and VMON monitors under the effect of the sextupole index in ARCF and ARCD ; the magnet centering is x_{off} (Eq. 8 and col. 3 of Table 1) (the original situation was the sextupole free case, Fig. 4). *Right plot* : the closed orbit in presence of fringe fields remains negligible and very similar to the sextupole free one.

Table 5: Machine tunes obtained by ray-tracing of paraxial rays. See Table 3 for comparison with the sextupole free machine.

	Horizontal tune	Vertical tune
Ray-tracing		
Sharp edge	0.430262	*0.413453* [a]
Fringe field	0.445824	0.395854

[a] Absence of fringe field compensated by wedge kick

Chromaticities are computed from tunes of particles launched on off-momentum closed orbit. We take $\delta p/p = 10^{-3}$ with chromatic closed orbit coordinates $x_{ch} = \eta_x \delta p/p \approx 1.975\ 10^{-3}$ m and $x'_{ch} = \eta'_x \delta p/p \approx 0.8\ 10^{-6}$ rad at the start of the structure [9]. This gives :

- Sharp edge model :

With sharp edge field model we obtain $\nu_x/\nu_y = 0.427924$ / 0.411289 which, given the on-momentum tunes 0.430262 / 0.413453 (Table 5) leads to $\delta\nu_{x,y}/\delta p/p$, $\delta\nu_{x,y}/\delta p/p =$ -2.34, -2.16 which compares fairly well with MAD values -2.36, -2.18 (App. C).

- Fringe field model :

In presence of fringe fields we get $\nu_x/\nu_y = 0.44368$ / 0.39367 which, given the on-momentum tunes 0.445824 / 0.395854 (Table 5) leads to $\delta\nu_{x,y}/\delta p/p$, $\delta\nu_{x,y}/\delta p/p =$ -2.14, -2.18 which does not differ much from the sharp edge model values above.

5 Conclusion

Effects of fringe fields in the Recycler combined function dipoles on machine tunes and other parameters have been investigated by means of stepwise ray-tracing.

In the sharp edge field model ray-tracing and matrix transport (MAD) give tune values similar at better than $\approx 3.3\ 10^{-4}$.

The ray-tracing reveals that tunes change by $\Delta\nu_x/\Delta\nu_y \approx 1.56\ 10^{-2}/-1.80\ 10^{-2}$ when fringe fields are set, both with and without sextupole index.

As a by-product of the study it has been shown that there is some sextupole feed down which entails additional tune increase by $\Delta\nu_x/\Delta\nu_y \approx 2.2\ 10^{-3}/3.1\ 10^{-3}$ w.r.t. the pure quadrupole case.

It has also been shown that the effects of fringe fields on magnet centering are negligible, as well as on such other machine parameters as Twiss functions and chromaticities. The horizontal closed orbit excursion due to fringe fields does not exceed $\pm 40\ \mu m$.

This work as benefited from numerous discussions, with N. Gelfand, J. Holt, F. Ostiguy and W. Wan, FNAL.

A Appendix. Input data to Zgoubi for ARCF and ARCD dipoles

Magnetic field values are computed from strengths $BARCK1F = 1.151435\,10^{-2}$, $BARCK1D = -1.111505\ 10^{-2}$, $BARCK2F = 1.155289\ 10^{-2}$, $BARCK2D = -1.942155\ 10^{-2}$ for 8 GeV protons ($B\rho = 29650.144531\ Tm$).

```
'MULTIPOL' RBEN      ARCF
0  .Dip               B0           B1           B2
  449.5800 10.00 1.3751329482 0.3414021432 0.0171272433 0.0 0.0 0.0 0.0 0.0 0.0 0.0
8.00  5.0  1.000 1.00 0.00 0.00 0.00 0. 0. 0. 0.
4  0.09650  3.76444 -0.70378  1.31734  0. 0.  0.
8.00  5.0  1.000 1.00 0.00 0.00 0.00 0. 0. 0. 0.
4  0.09650  3.76444 -0.70378  1.31734  0. 0.  0.
 0. 0. 0. 0. 0. 0. 0. 0. 0. 0.
120.080E10  Dip
3  0.   7.8426319361E-01  1.0425639339E-02

'MULTIPOL' RBEN      ARCD
0  .Dip               B0           B1            B2
  449.5800 10.00 1.3751329482 -0.3295628726 -0.0287925894 0.0 0.0 0.0 0.0 0.0 0.0 0.0
8.00  5.0  1.000 1.00 0.00 0.00 0.00 0. 0. 0. 0.
4  0.09650  3.76444 -0.70378  1.31734  0. 0.  0.
8.00  5.0  1.000 1.00 0.00 0.00 0.00 0. 0. 0. 0.
4  0.09650  3.76444 -0.70378  1.31734  0. 0.  0.
 0. 0. 0. 0. 0. 0. 0. 0. 0. 0.
120.080E10  Dip
3  0.   7.7828419209E-01  1.0425639339E-02
```

B Appendix. Difference between cosine-like and circular paths

The equation of the ρ-circular path $x_c(z)$ tangent to the cosine-like trajectory x(z) (Eq. 11) at entrance and exit of the magnet (Fig. 2) is

$$(x_c + \rho cos\frac{\theta}{2})^2 + (z_c - L_{mag}/2)^2 = \rho^2 \tag{15}$$

The difference $x(z) - x_c(z)$ is shown in Fig. 7.

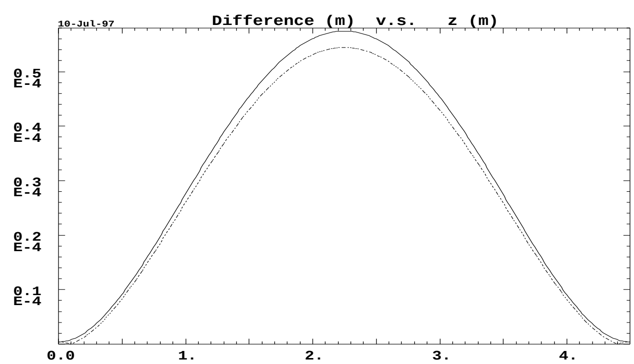

Figure 7: Difference between cosine-like and circular paths as a function of longitudinal coordinate z in ARCF and ARCD..

C Appendix. MAD data, modified dipole

Note in the following that, on the one hand the dipole length has been changed to the arc length (w.r.t. the original data [9]), on the other hand a correction wedge angle has been introduced at both ends of the dipoles to account for the varying bending radius (App. D).

Recycler dipoles data

```
dir:= -1   ! for protons
barcang~:= twopi/(301. + 1./3.)*dir
lbarcmag~:=  4.4958              !(177")
ldip    = lbarcmag /(2.*sin(barcang/2.)) * barcang
BARCK1F   =   1.151435E-02         ;         BARCK1D   =  -1.111505E-02
BARCK2F =     1.155289E-02*dir     ;        BARCK2D =    -1.942155E-02*dir

ARCF:  RBEND, TYPE=arcf, L=ldip, ANGLE = barcang, K1= barck1f, K2= sk2 * barck2f, fint= FF*.234, &
                    hgap=.025, e1 = -wcor*arcf[k1]*(arcf[L])^2*arcf[angle]/24., e2 = arcf[e1]
ARCD:  RBEND, TYPE=arcd, L=ldip, ANGLE = barcang, K1 = barck1d, K2= sk2* barck2d, fint= FF*.234, &
                    hgap=.025, e1 = -wcor*arcd[k1]*(arcd[L])^2*arcd[angle]/24., e2 = arcd[e1]
DISF:  RBEND, TYPE=disf, L=2./3.*ldip, ANGLE= bdisang, K1=bdisk1f, fint= FF * .234, hgap=.025   ,&
                e1 = -wcor*disf[k1]*(disf[L])^2*disf[angle]/24., e2 = disf[e1]
DISD:  RBEND, TYPE=disd, L=2./3.*ldip, ANGLE = bdisang, K1= bdisk1d,fint= FF * .234, hgap=.025  ,&
                e1 = -wcor*disd[k1]*(disd[L])^2*disd[angle]/24., e2 = disd[e1]
```

Machine parameters - Sharp edge, no wedge correction

FF = 0 and wcor = 0, in dipole data above

```
ARCF matrix                                        ARCD matrix
     0.885870    4.323187    0.000000    0.000000        1.114453    4.665796    0.000000    0.000000
    -0.049786    0.885870    0.000000    0.000000        0.051868    1.114453    0.000000    0.000000
     0.000000    0.000000    1.118418    4.672317        0.000000    0.000000    0.889544    4.329416
     0.000000    0.000000    0.053691    1.118418        0.000000    0.000000   -0.048208    0.889544

Machine parameters
 ------------------------------------------------------------------------------------------------------------------------
     ELEMENT SEQUENCE       I                H O R I Z O N T A L                I                 V E R T I C A L
 pos.  element occ.      dist I    betax  alfax    mux     x(co)  px(co) Dx     Dpx  I   betay  alfay    muy    y(co)  py(co) Dy     Dpy
 no.   name    no.        [m]  I    [m]    [1]      [2pi]  [mm]   [.001] [m]    [1]  I   [m]    [1]      [2pi]  [mm]   [.001] [m]    [1]
 ------------------------------------------------------------------------------------------------------------------------
 begin RING       1      0.000    52.179 -0.031    0.000  0.000   0.000  1.976 0.001    13.076 -0.001   0.000  0.000  0.000  0.000 0.000
 end   RING       1   3319.423    52.179 -0.031   25.428  0.000   0.000  1.976 0.001    13.076 -0.001  24.411  0.000  0.000  0.000 0.000
 ------------------------------------------------------------------------------------------------------------------------
 total length =       3319.422902          Qx            =         25.427659          Qy            =         24.410599
 delta(s)     =          0.000000 mm       Qx'           =         -2.362489          Qy'           =         -2.185484
 alfa         =          0.242367E-02      betax(max)    =         55.998905          betay(max)    =         54.326249
 gamma(tr)    =         20.312475          Dx(max)       =          1.993019          Dy(max)       =          0.000000
                                           Dx(r.m.s.)    =          1.248686          Dy(r.m.s.)    =          0.000000
                                           xco(max)      =          0.000000          yco(max)      =          0.000000
                                           xco(r.m.s.)   =          0.000000          yco(r.m.s.)   =          0.000000
 ------------------------------------------------------------------------------------------------------------------------
```

Machine parameters - Sharp edge, wedge correction

FF = 0 and wcor = 1, in dipole data above

```
ARCF matrix                                        ARCD matrix
     0.885866    4.323187    0.000000    0.000000        1.114457    4.665796    0.000000    0.000000
    -0.049788    0.885866    0.000000    0.000000        0.051870    1.114457    0.000000    0.000000
     0.000000    0.000000    1.118423    4.672317        0.000000    0.000000    0.889540    4.329416
     0.000000    0.000000    0.053693    1.118423        0.000000    0.000000   -0.048209    0.889540

Machine parameters
 ------------------------------------------------------------------------------------------------------------------------
     ELEMENT SEQUENCE       I                H O R I Z O N T A L                I                 V E R T I C A L
 pos.  element occ.      dist I    betax  alfax    mux     x(co)  px(co) Dx     Dpx  I   betay  alfay    muy    y(co)  py(co) Dy     Dpy
 no.   name    no.        [m]  I    [m]    [1]      [2pi]  [mm]   [.001] [m]    [1]  I   [m]    [1]      [2pi]  [mm]   [.001] [m]    [1]
 ------------------------------------------------------------------------------------------------------------------------
 begin RING       1      0.000    52.173 -0.032    0.000  0.000   0.000  1.975 0.001    13.073 -0.001   0.000  0.000  0.000  0.000 0.000
 end   RING       1   3319.423    52.173 -0.032   25.428  0.000   0.000  1.975 0.001    13.073 -0.001  24.411  0.000  0.000  0.000 0.000
 ------------------------------------------------------------------------------------------------------------------------
 total length =       3319.422902          Qx            =         25.428346          Qy            =         24.411267
 delta(s)     =          0.000000 mm       Qx'           =         -2.353590          Qy'           =         -2.196583
 alfa         =          0.242352E-02      betax(max)    =         56.002880          betay(max)    =         54.322507
 gamma(tr)    =         20.313115          Dx(max)       =          1.992772          Dy(max)       =          0.000000
                                           Dx(r.m.s.)    =          1.248608          Dy(r.m.s.)    =          0.000000
                                           xco(max)      =          0.000000          yco(max)      =          0.000000
                                           xco(r.m.s.)   =          0.000000          yco(r.m.s.)   =          0.000000
 ------------------------------------------------------------------------------------------------------------------------
```

Machine parameters - With fringe fields and wedge correction
FF = 1 and wcor = 1, in dipole data above

```
ARCF matrix                                                   ARCD matrix
     0.885866    4.323187    0.000000    0.000000                  1.114457    4.665796    0.000000    0.000000
    -0.049788    0.885866    0.000000    0.000000                  0.051870    1.114457    0.000000    0.000000
     0.000000    0.000000    1.118424    4.672317                  0.000000    0.000000    0.889541    4.329416
     0.000000    0.000000    0.053693    1.118424                  0.000000    0.000000   -0.048209    0.889541

 Machine parameters
--------------------------------------------------------------------------------------------------------------------------------
     ELEMENT SEQUENCE       I                   H O R I Z O N T A L                 I                  V E R T I C A L
pos.  element occ.      dist I    betax  alfax    mux    x(co)   px(co) Dx     Dpx  I   betay  alfay    muy    y(co)  py(co) Dy     Dpy
no.   name    no.        [m]  I    [m]    [1]     [2pi]  [mm]    [.001] [m]    [1]  I    [m]    [1]     [2pi]  [mm]   [.001] [m]    [1]
--------------------------------------------------------------------------------------------------------------------------------
begin RING       1     0.000    52.173 -0.032   0.000  0.000  0.000  1.975 0.001   13.074 -0.001   0.000  0.000  0.000  0.000 0.000
end   RING       1  3319.423    52.173 -0.032  25.428  0.000  0.000  1.975 0.001   13.074 -0.001  24.411  0.000  0.000  0.000 0.000
--------------------------------------------------------------------------------------------------------------------------------
total length =       3319.422902          Qx          =         25.428346          Qy          =         24.410859
delta(s)     =          0.000000 mm       Qx'         =         -2.353590          Qy'         =         -2.195833
alfa         =          0.242352E-02      betax(max)  =         56.002880          betay(max)  =         54.323727
gamma(tr)    =         20.313115          Dx(max)     =          1.992772          Dy(max)     =          0.000000
                                          Dx(r.m.s.)  =          1.248608          Dy(r.m.s.)  =          0.000000
                                          xco(max)    =          0.000000          yco(max)    =          0.000000
                                          xco(r.m.s.) =          0.000000          yco(r.m.s.) =          0.000000
--------------------------------------------------------------------------------------------------------------------------------
```

D Appendix. Correction of the wedge angle in matrix transport for the effect of the non-constant bending. Effect on tunes.

When using RBEND, MAD assumes the entrance and exit wedge angle focusing term to be $\tan(\theta/2)/\rho$ with $\rho = L/\theta$ while it should be

$$\frac{\tan(\theta/2)}{\rho_{off}} \approx \frac{\tan(\theta/2)}{\rho}(1 - \frac{\rho_{off} - \rho}{\rho}) = \frac{\tan(\theta/2)}{\rho} - \frac{\rho_{off}}{\rho}) \tan(\theta/2) \tag{16}$$

RBEND must therefore be given a correction wedge angle ϵ such that $\tan\epsilon = (1 - \frac{\rho_{off}}{\rho})\tan(\theta/2)$. From Eq. 10 we get

$$\rho_{off} = \frac{1}{Kx_{off}} \approx (1 + \frac{KL^2}{12})\rho, \quad 1 - \frac{\rho_{off}}{\rho} \approx -\frac{KL^2}{12} \tag{17}$$

Considering that ϵ and θ are small quantities leads to the entrance and exit correction wedge angle

$$\epsilon \approx \frac{-KL^2\theta}{24} \tag{18}$$

The effect of this correction is as follows. In ARCF/DISF K positive entails $\epsilon < 0$ and actual wedge angle $< \theta/2$, hence the horizontal (vertical) focusing tends to increase (decrease) w.r.t. a rectangular BEND, and conversely in ARCD/DISD : $K < 0$, $\epsilon > 0$, actual wedge angle $> \theta/2$, hence decreased (increased) horizontal (vertical) focusing. The overall effect on tunes is a balance between the two opposing trends, given at first order by

$$\Delta\nu = \frac{1}{4\pi}\int_{ARCF} \beta_F \Delta K_F ds + \frac{1}{4\pi}\int_{ARCD} \beta_D \Delta K_D ds \tag{19}$$

with $\int \Delta K_{F/D} ds \approx -\frac{\epsilon_{F/D}}{\rho} \approx K_{F/D}L^2\theta/24\rho \approx +9.4\ 10^{-7}/-9.1\ 10^{-7}$. If we take $\beta_{F/D} \approx 50$ m in ARCF/D and ≈ 30 m in DISF/D and neglect the effect of defocusing dipoles, the equation above gives $\Delta\nu \approx 8\ 10^{-4}$ which compares fairly well with MAD simulations (App. C) : ν_x/ν_z change by $7\ 10^{-4}$ from 25.427659/24.410599 without correction to 25.428346/24.411267 if a correction is set.

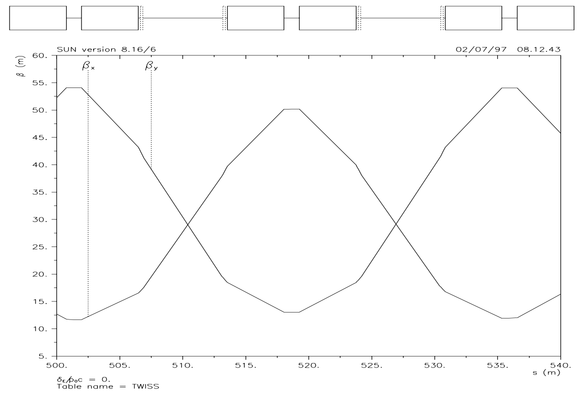

Figure 8: β functions in arc cell.

E Appendix. Sextupole feed down to quadrupole

We estimate the effect of sextupole feed down on tunes in terms of $\Delta\nu = (1/4\pi)\int \beta\Delta K ds$. The β functions reach a maximum in any focusing type dipole (ARCF for horizontal motion and ARCD for vertical) and behave symmetrically in in a half-cell since there are 2 dipoles per half-cell (Fig. 8). This allows to write for both x and y motions

$$\beta(z) = cos^2(z\sqrt{(K)})\beta_{max} + sin^2(z\sqrt{(K)})/\beta_{max} \quad (K \gtrless 0) \tag{20}$$

inside any focusing dipole. After some algebra, and neglecting the effect of defocusing type dipoles (ARCF in the vertical plane and ARCD in the horizontal) one gets

$$\Delta\nu \approx \frac{N}{4\pi}\int \beta(z)\Delta K(z)dz = \frac{2NH}{4\pi}\frac{C}{K}(\beta_{max} - \frac{1}{K\beta_{max}})\{\frac{2}{3}(1+\frac{C}{2}) - \frac{S}{L}\} \tag{21}$$

with $C = cos(L\sqrt{K})$, K = quadrupole strength, H = sextupole strength. Given N=108 dipoles, $\beta_{max} \approx 55$ we get $\Delta\nu_x/\Delta\nu_y \approx 2.3\,10^{-3}/3.8\,10^{-3}/$ which is close to the change observed $(2.15\,10^{-3}/3.1\,10^{-3})$ when setting the sextupole index (Tables 3, 5).

References

[1] Fermilab Recycler ring TDR, G. Jackson Ed., FERMILAB-TM-1981, July 1996.

[2] F. Méot and S. Valéro, Zgoubi users' guide, Note CEA/DSM/LNS/GECA/97-43 and FERMILAB-TM-2010, CEA-Saclay and FNAL, 1997.

[3] F. Méot, A numerical method for the ray-tracing of polarized beams, Proc. EPAC Conf. 1992.

[4] F. Méot, On the effects of fringe fields in the LHC ring, Part. acc., 1996, Vol. 55, pp.[329-338]/83-92 ; F. Méot, A. París, On the effect of high-β region fringe fields and multipole errors in LHC, FNAL, 1997, to be published.

[5] G. Leleux, Compléments sur la physique des accélérateurs, DEA de Physique et Technologie des Grands Instruments, rapport CEA/DSM/LNS/86-101, CEA, Saclay (1986).

[6] H.A. Enge, Deflecting magnets, in *Focusing of charged particles*, volume 2, A. Septier ed., Academic Press, New-York and London (1967).

[7] Fringe field data provided by J.F. Ostiguy, BD/Phys., FNAL, 1997.

[8] H. Grote and F.C. Iselin, The MAD program V8.10, CERN/SL/90-13 (AP) (1993).

[9] MAd file rrv11d.lat, provided by J. Holt, BD/Phys., FNAL, 1997.

[10] N. Gelfand, Rectangular combined function magnets, Report MI-0200, FNAL, Jan. 1997.

[11] S. D. Holmes, Reference orbit trajectory in a combined function magnet, Report MI-0195, FNAL, Dec. 1996.